RYERSON UNIVERSITY

Final Report

ORF-RE Project – Future Urban Electric System Project

(Theme 2, Part 1)

Analysis, Design and Implementation of Bidirectional Fast Charger for Plug-in Hybrid Electric Vehicles (PHEV)

For

Toronto Hydro Electric System Limited (THESL)

and

Centre for Urban Energy (CUE)

Prepared by

L. Tan, S. Rivera, V. Yaramasu, J. Wang, and B. Wu

Department of Electrical and Computer Engineering

Ryerson University

July 10, 2015

Table of Contents

1 Introduction

As viable alternatives to conventional internal combustion engine vehicles (ICEVs), the plug-in hybrid electric vehicles (PHEVs) and electric vehicles (EVs) are increasing their market share gradually because of decreased fossil fuels consumption and reduced greenhouse gas emissions [1]. Surveys indicate that the range per charge, the charging time, the available charging facilities are the greatest concerns of consumers, which are also the main factors influencing their purchase of EVs [2]. In order to allow the future widespread use of EVs [3], [4], there is an urgent demand to develop fast chargers to shorten the charging time, and to deploy the high-power charging stations infrastructure to alleviate range anxiety for drivers. If fast chargers reduce the EVs replenishing time within acceptable levels comparable to the usual refueling of ICEVs, and the high-power charging stations spread all over the cities and highways as the gas stations do, the acceptance of EVs will be greatly enhanced [1-5].

2 PHEV Charging Levels

Charging of the PHEV batteries can be carried out either conductively or inductively. Conductive charging transfers the energy into the EV battery pack through electrical contact between the charge port of the vehicle and the charger connector, whereas inductive charging makes use of wireless energy transfer through electromagnetic field coupling to eliminate the plug-in cord. At present, the inductive charging remains a developing technology with some prototypes built and tested at a few R&D facilities. On the other hand, the conductive charging is already adopted by the EV industry including mainstream EV manufacturers. Depending on the rate at which the EV battery is charged, conductive chargers can be generally classified into slow chargers and fast chargers; the charging levels are defined in the existing EV standards.

2.1 SAE J1772 Standard

Table 1. Charging levels defined in Society of Automotive Engineers (SAE) J1772 standard [6]

Level	Current	Electric Potential Difference (V)	Current (A)	Power (kW)	BEV Charging Time** (minutes)			
					3.3kW charger	7kW charger	20kW charger	45kW charger
Level 1	AC	120	12/16	1.4/1.92	1,020			
Level 1	DC	200-450	80	36	-	-	72	-
Level 2	AC	240	80	19.2	420	210	72	-
Level 2	DC	200-450	200	90	-	-	-	20
Level 3*	DC	200-600	400	240	-	-	-	<10

* There is no official Level 3 today. This is the proposed standard by the SAE.

** Assumes 25 kWh of usable capacity beginning at 20 percent state of charge (SOC). If power provided can charge the battery in less than one hour, then charging stops at 80 percent SOC. AC charging uses an on-board charger. DC charging uses an off-board charger.

As outlined in Table 1, the latest version of **SAE J1772** standard [7] developed by Society of Automotive Engineering (SAE) has included three charging levels:

a) Level I: on-board charger, AC voltage 120V or 240 V with maximum current of 15 A (standard home outlet), maximum power of 3.3 kW.

b) Level II: on-board charger, AC voltage 240 V with maximum current of 60 A, maximum power of 14.4 kW.

c) Level III: off-board charger, DC voltage provided directly to the battery via a DC connector, not fully defined yet, potential maximum value of 600V/400A/240 kW.

Level I and II in general fall into the category of slow charging, with one exception being the Level II DC charging.

A European standard IEC 61851 has also been developed promoting different levels (up to 690V AC and 1000V DC) analogous to the SAE J1772, and coordination between the two standards is ongoing [8].

2.2 CHAdeMO Standard

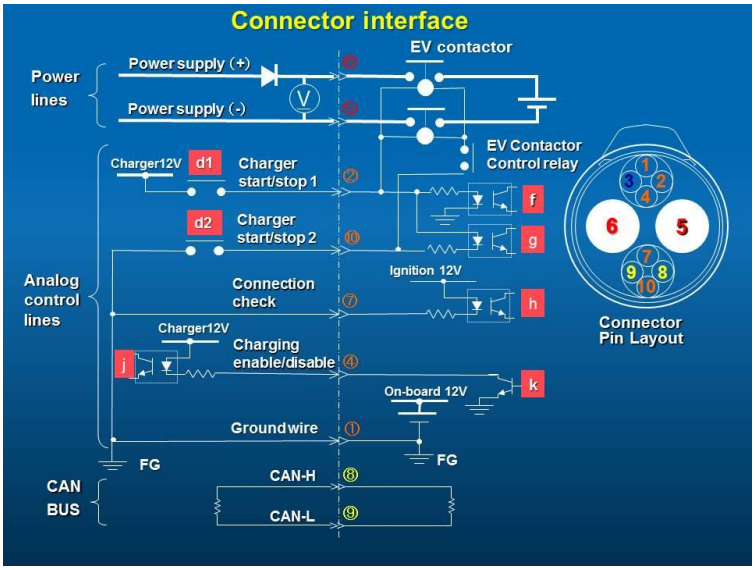

Figure 1. Connector interface definition as per CHAdeMO protocol.

Other than the SAE and IEC standards, an association named CHAdeMO proposed a quick charging method as a global industry standard. CHAdeMO is an abbreviation of “CHArge de MOve", equivalent to “charge for moving” [9].

CHAdeMO was formed by The Tokyo Electric Power Company (TEPCO), Nissan, Mitsubishi and Fuji Heavy Industries. Toyota later joined as its fifth executive member. Tokyo Electric Power Company has developed patented technology and a specification for high-voltage high-current automotive fast charging via a JARI DC fast charge connector. It appears as a basis for the CHAdeMO protocol. The connector is specified by the JEVS (Japan Electric Vehicle Standard) G105-1993 from the Japan Automobile Research Institute. The maximum output compatible with CHAdeMO protocol is 500V/125A/62.5kW.

3 Power Converter Based Fast Chargers

The power electronic converter for implementing a PHEV battery charger includes an AC-DC rectifier stage that converts AC grid power into DC form and a DC-DC stage for adapting to different battery voltage levels. The line-side AC-DC rectifier should be able to satisfy grid

harmonic restrictions as well as power factor requirement. In order to realize V2G function, the converter should be bidirectional to allow for regenerative operation. Moreover, the charger should have a galvanic isolation from the main distribution network to meet safety standards.

3.1 Power Electronic Converters

As was discussed before, fast charging structures allows the car batteries to be charged in the shortest possible time, allowing a "fuel stop" equivalent for EVs and PHEVs. These structures are based on power electronics solutions, which allow the energy transformation and distribution for charging purposes. **In order to provide a proper charging process, some basic requirements must be complied:**

- Universal supply: Considering the different kinds of vehicles (small cars to heavy vehicles), the batteries are in a wide range of specific-energy, from few kWh to several tens of kWh. **Thus, the charging station must be able to provide any DC output voltage in the range between 100-600 V. Also, depending on the battery characteristics, the converter must meet a specific charging profile.**
- "Fuel stop" equivalency: In order to provide a quick re-charge of the batteries in the EVs, **the station must be able to provide enough power to bring a high specific energy battery (30-40 kWh) to a state of charge (SOC) over 80% in less than 10 minutes**.
- Battery care: the charging process must be safe and secure for the battery set. This sets very tight values for both current and voltage ripple values**. In the first case, the maximum allowed ripple is 1% of the minimal value of the current output profile. The latter is specified to be lower than 5% of the maximum output voltage.**
- Galvanic isolation towards the utility grid: According to the existing standards, **the charging station must provide a full galvanic isolation towards the distribution grid.** This means, that the converter must include a transformer in its structure, which could be either a traditional grid frequency (low frequency) transformer or a high frequency transformer (included in the DC to DC conversion stage).
- Bidirectional power flow: As it may not be a primary requirement, considering the potential increase in the use of EVs and PHEVs, the utility grid is expected to have significant

reformations. The parked vehicles can support the grid as storage devices, and supply energy back to the grid during the peak hours, and then charged back during the off peak hours (considering that in most of the cases a vehicle passes most of the time parked [5]). To allow both grid to vehicle (G2V) and vehicle to grid (V2G) operations, **bidirectional converters should be used.**

3.2 Fast Charging Techniques

One of the key features of fast charging is the high power levels of the operation, allowing a quick energy transfer into the battery. The power level will be determined not only by the battery chemistry, but also by the method used for charging it. In order to reduce the charging times, and offer a secure and reliable charging several techniques have been studied and developed [10]. The method presented in Figure 2, is called constant current – constant voltage (CC-CV), and its basic idea is to charge the battery with a constant DC current (specified by the cell manufacturer), until it reaches a certain voltage. After reaching this point, the charging process is switched to constant voltage mode. The battery is charged at CV until the current draw drops to the cut off value, making the charging process complete. This method is widely used in EV and PHEV battery charging.

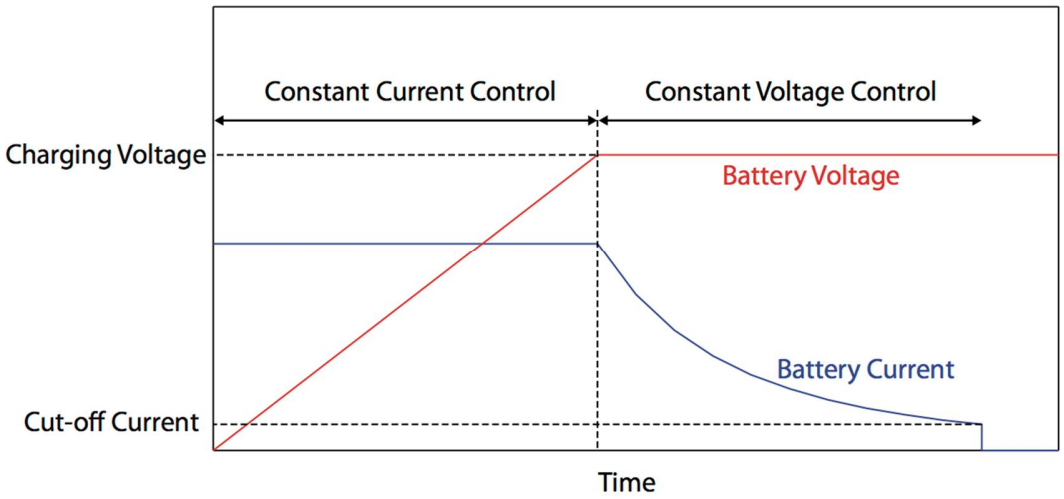

Figure 2. Battery voltage and current during CC and CV charging profiles.

Other charging methods based on the CC-CV have been developed to increase the charge acceptance rate of the battery, such as the multistage constant current – constant voltage (MCC-CV) or the negative pulse CC-CV.

3.3 Proposed Configurations

In order to meet the mentioned requirements, and based on the galvanic isolation solution selected, it is possible to find two different approaches in the literature [10, 11]. The first uses a transformer as an interface of the charging station with the grid, while the latter includes an isolated DC-DC conversion stage. In the following section both configurations will be fully described and compared, in order to highlight its advantages and drawbacks.

3.3.1 Low-Frequency Configuration

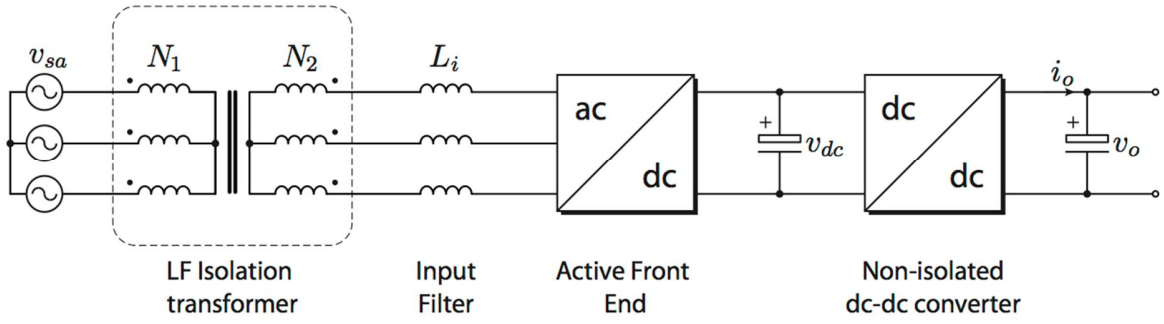

Figure 3. Charging station and fast charger configuration with low-frequency isolation.

The layout of the low-frequency charging station is presented in Figure 3. The power conversion system consists of four major parts: 1) an input line-frequency transformer, providing galvanic isolation between the charging station and utility grid; 2) a harmonic filter to reduce the AC currents harmonic distortion such that the IEEE and IEC standards are met; 3) a three-phase active rectifier which controls net DC-bus voltage and grid reactive power (power factor); and 4) a DC-DC stage, which regulates the DC output (voltage and current) in order to meet the battery charging profile.

The advantage of this topology is the use of a conventional line frequency transformer, which is simple and does not need a complex design process. The use of transformer-less DC-DC conversion stages provides flexibility in the configuration selection, and if needed interleaving several DC-DC stages can be used in order to decrease the output current ripple, thereby reducing the size of DC-DC converter output filter.

On the other hand, the need of larger magnetic materials increases the size and weight of the low-frequency transformer. To reduce switching losses and reverse recovery losses, the power converters should operate at lower switching frequency. The low switching frequency operation increases the harmonic filter size, in addition to the low dynamic control response.

3.3.2 High-Frequency Configuration

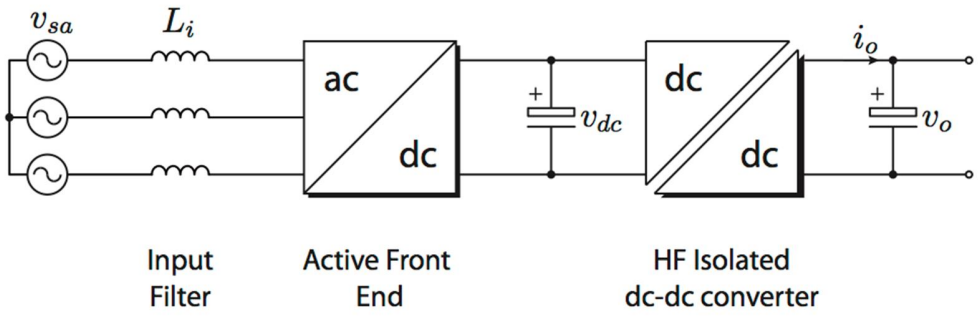

Figure 4. Charging station and fast charger configuration with high-frequency isolation.

A high-frequency galvanic isolation architecture is presented in Figure 4. The system is comprised by three main parts: 1) input harmonic filter; 2) three phase active rectifier, providing the same functions as in the LF architecture; and 3) isolated DC-DC conversion stage, which provides the galvanic isolation in addition to controlling the DC output.

Because of the high operating switching frequency of the transformer, this architecture allows to reduce the volume and weight of the charging system (resulting in a much higher power density of the system), also the HF transformer properly shapes the output current, reducing the size of the DC-DC converter output filter.

However, this configuration needs parallel connection of several DC-DC stages in order to reduce the output ripple and to meet the current charging profile (reduce the current conducted by the switching devices). Also the transformer implies a complex design and a higher cost compared with the LF solution, as it might need special magnetic cores (amorphous alloy or nanocrystalline).

3.3.3 Interleaved Buck Converter

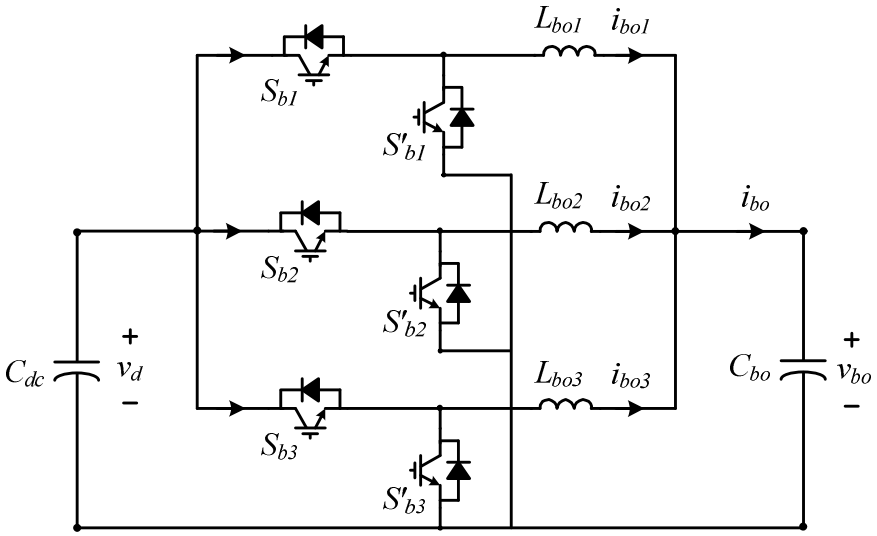

Figure 5. Bidirectional fast charger topology based on the three-phase interleaved synchronous buck converter.

Since a line-frequency transformer is employed at grid-side for voltage step-down purpose, the LF isolation based charging station architecture is selected, where the power circuit for fast chargers can use non-isolated topologies. Figure 5 presents the topology of a three-phase interleaved buck converter, in which each branch or phase operates in similar manner, with a phase shift of $2\pi/3$ [rad]. Such operation will have a multiplicative effect on the output frequency due to a harmonic cancellation between the branches. This is demonstrated as follows: consider that each converter branch circulates a current i_{Lj}, where $j = (a, b, c)$. These currents have a triangular waveform. They are expressed as follows:

$$i_{Lj}(t) = I_0 + \sum_{n=1}^{\infty} I_n \sin\left(n\omega_s t + \theta_j\right), \quad (1)$$

where $\omega_s = 2\pi f_s$, f_s is the switching frequency of the buck converter, and I_n is defined as

$$I_n = -\frac{2(-1)^n}{n^2 D(1-D)\pi^2}\frac{\Delta i_L}{2}\sin(n(1-D)\pi), \tag{2}$$

where D is the duty cycle and $\Delta i_L = \frac{v_o(1-D)}{L_o f_s}$ is the branch current ripple. The output current i_o is the sum of all the converter branch currents. With this condition, all the harmonics with order $6n \pm 1$ are cancelled for any duty cycle and are not transferred to the load (considering a balanced operation for interleaved branches). This leads to lower output current ripple as demonstrated below [12], [13]:

$$\Delta i_o = \frac{v_i D}{L_o f_s}\left[1 - \frac{\text{floor}(3D)}{3D}\right][1 + \text{floor}(3D) - 3D], \tag{3}$$

4 DC-DC Charger Control

4.1 Controller Structure

The DC-DC charger control has two control loops: 1) outer battery voltage control loop, and 2) inner DC-DC converter output current control loop. The DC-DC charger stage requires different modes of control, such as CC or CV for battery charging. In CC mode, the reference is given directly to the current regulator input; while in the CV mode, the battery voltage regulator provides the current reference for inner current control loop. The basic control structure with the aforementioned features is illustrated in Figure 6.

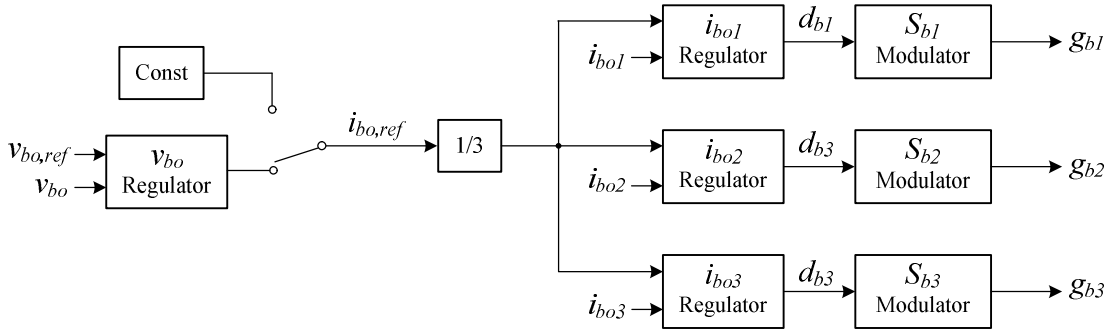

Figure 6. Overall control scheme for interleaved DC-DC converter stage.

4.2 Buck Converter Current Control

The inner current loop design of the DC-DC buck stage is similar to that of the grid-side VSCs. Figure 7 demonstrates that the equivalent transfer function of the three buck converter current control loops is the same as that of any individual one**.**

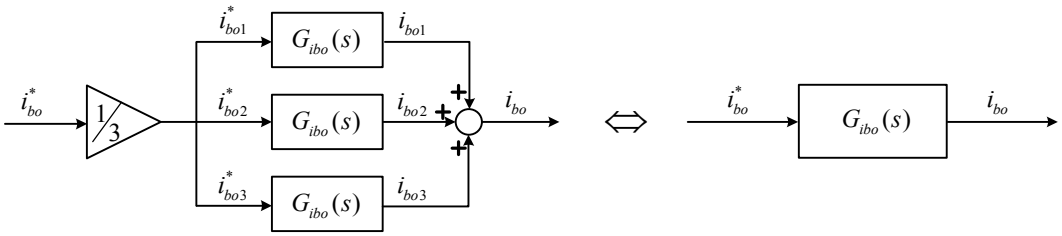

Figure 7. Individual and equivalent transfer functions for multiple buck converter.

To ensure a stable DC voltage, the current loop bandwidth is limited to 1/5 of the DC voltage control loop bandwidth.

$$f_{c\_ibo}(s) = \frac{1}{5} f_{c\_vdc} = 20Hz \tag{4}$$

The block diagram for active current control loop is shown in Figure 8. To ensure enough gain at low speed for CC mode control, the compensator has the form of both proportional and integral (PI) terms. Thus,

$$\begin{aligned} G_{openl\_ibo}(s) &= G_{c\_ibo}(s) G_{ibo\_vlbo}(s) H_{f\_ibo}(s) \\ &= \left(k_{p\_ibo} + \frac{k_{i\_ibo}}{s} \right) \times \frac{1}{sL_{bo}} \times \frac{2\pi f_{c\_ibo} \times 10}{s + 2\pi f_{c\_ibo} \times 10} \end{aligned} \tag{5}$$

The desired performance can be obtained with the following PI parameters. With the help of Figure 9, the phase margin is measured as 69^o.

$$k_{p\_ibo} = 0.0015 \quad \text{and} \quad k_{i\_ibo} = 0.05 \tag{6}$$

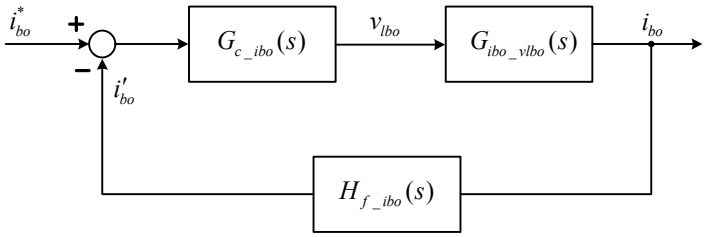

Figure 8. Block diagram of active current control loop.

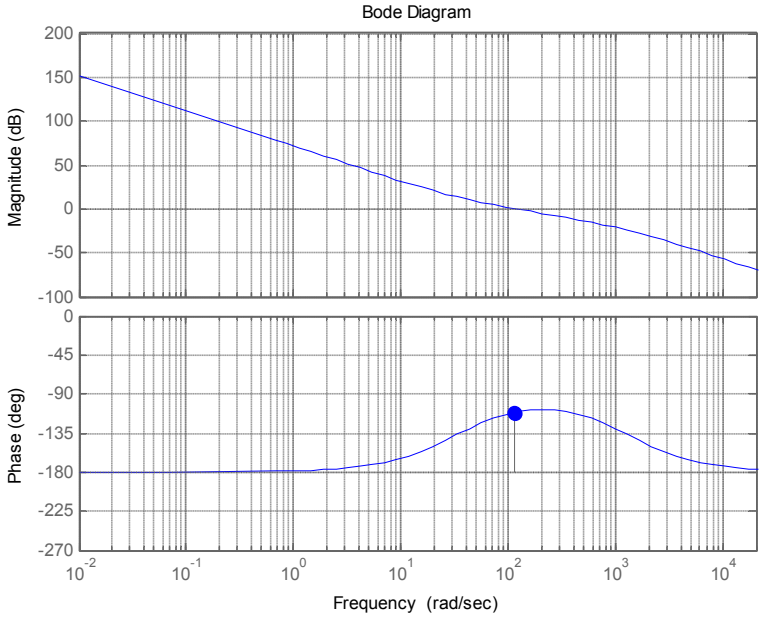

Figure 9. Bode plot diagram for buck converter current control open-loop transfer function

4.3 Battery Voltage Control

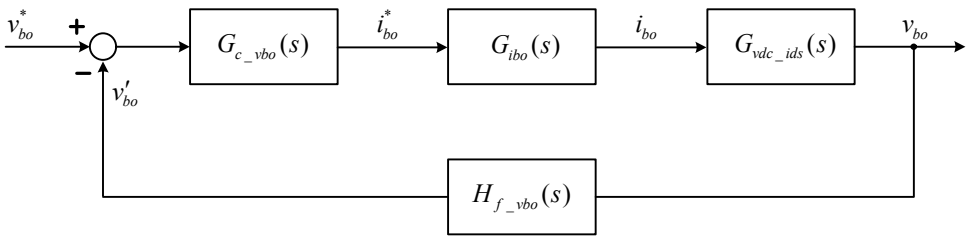

Figure 10. Block diagram of battery voltage control loop.

The simplified battery voltage controller structure is shown in Figure 10. Similarly, the inner current loop is approximated as a low pass filter,

$$G_{ibo}(s) = \frac{2\pi f_{c\_ibo}}{s + 2\pi f_{c\_ibo}} \tag{7}$$

To derive the transfer function of $G_{vbo\_ibo}(s)$, the following converter dynamics are considered:

$$L_{bo} \frac{di_{bo}}{dt} = dv_{dc} - v_{bo} \tag{8}$$

$$C_{bo} \frac{dv_{bo}}{dt} = i_{bo} - i_{bat} \tag{9}$$

Also, the battery can be simplified as an ideal voltage source in series with a resistance, as shown in Figure 11. Therefore,

$$i_{bat} = \frac{v_{bo} - v_{bat}}{r_{bat}} \tag{10}$$

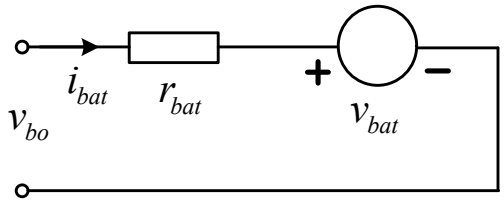

Figure 11. Equivalent circuit of battery model for transfer function studies.

By applying small-signal modeling to the above converter models, and by linearizing the system at a steady-state operating point, we have,

$$L_{bo} \frac{d\triangle i_{bo}}{dt} = \triangle v_{bo} \tag{11}$$

$$C_{bo} \frac{d\triangle v_{bo}}{dt} = \triangle i_{bo} - \frac{\triangle v_{bo}}{r_{bat}} \tag{12}$$

The disturbances on battery voltage, buck converter duty cycle, and input DC voltage are neglected. With Laplace transformation, we have

$$sC_{bo}v_{bo}(s) = i_o(s) - \frac{v_{bo}(s)}{r_{bat}} \tag{13}$$

And thus the plant transfer function is derived as,

$$G_{vbo\_ibo}(s) = \frac{r_{bat}}{sr_{bat}C_{bo}+1} \tag{14}$$

The open-loop transfer function for the battery voltage control loop is then,

$$\begin{aligned} G_{openl\_vbo}(s) &= G_{c\_vbo}(s)G_{ibo}(s)G_{vbo\_ibo}(s)H_{f\_vbo}(s) \\ &= \left(k_{p\_vbo} + \frac{k_{i\_vbo}}{s}\right) \times \left(\frac{2\pi f_{c\_ibo}}{s + 2\pi f_{c\_ibo}}\right) \times \left(\frac{r_{bat}}{sr_{bat}C_{bo}+1}\right) \times 1 \end{aligned} \tag{15}$$

The DC voltage loop is designed to have a bandwidth of approximately 2 Hz. The values of compensator to provide the desired performance are given in (16). The phase margin is around 92 degree, as shown in the bode plot in Figure 12.

$$k_{p\_vbo} = 3.5 \quad \text{and} \quad k_{v\_ibo} = 330 \tag{16}$$

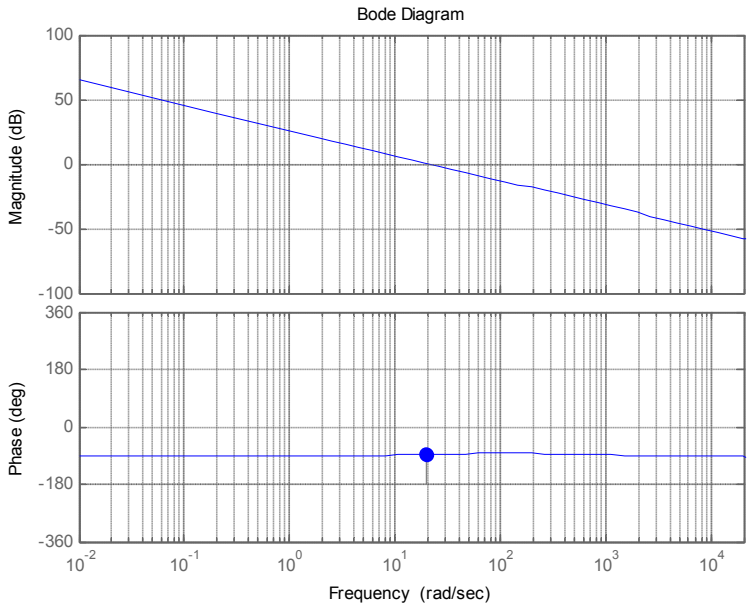

Figure 12. Bode plot diagram for the battery voltage control loop open-loop transfer function.

5 Simulation and Experimental Verification

5.1 Output Filter Design for a 240 kW 3-Phase Interleaved Buck Converter.

1) Output Inductor Design

The fast charger is designed to have a rated power of 240 kW, and a DC output voltage in the range of 100-600 V. The system will be connected to a utility grid with a line to line voltage of 690 V (rms). The input DC voltage is assumed to be 1000 V (half of the total DC bus voltage 2000 V) which is provided by an active front-end rectifier. Considering the high power rating of fast charger, the switching frequency for the DC-DC conversion stage is fixed at 2 kHz. The power converter system output will guarantee the charging current profile presented in Figure 13 (a).

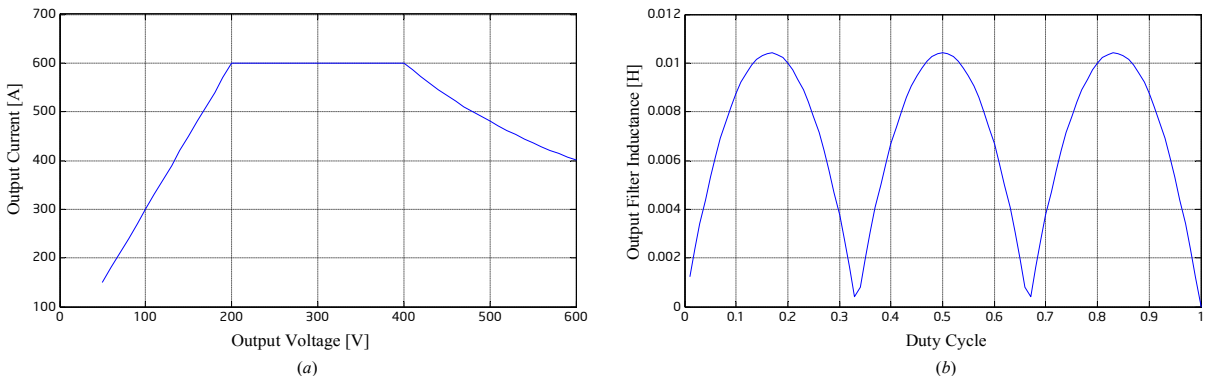

Figure 13. a) output current profile for 240kW fast charger; b) minimal phase inductor value at a switching frequency of 2 kHz.

In order to design the output filter values, equation (1) is revisited. Considering the requirement for the current ripple (1% of the minimal current in the output profile), and the output profile achieved at 2 kHz, the inductance value is given by

$$L_o = \frac{v_i D}{\Delta i_o f_s}\left[1 - \frac{\text{floor}(3D)}{3D}\right][1 + \text{floor}(3D) - 3D]\,. \tag{17}$$

Figure 13 (b) shows the inductance variation in the voltage output range. It is clear that L_o reaches its maximum value for $D = \frac{j}{6}, j = (1,3,5)$, with a peak value of $10.4\ mH$.

2) Output Capacitor Design

The output capacitor is chosen following a simple energy balance equation. The capacitor delivers the energy to the load during half cycle of the output frequency, so the energy change is,

$$\Delta E_1 = \int_{\frac{T_{on}}{2}}^{T_s - \frac{T_{off}}{2}} \Delta P_c dt = \frac{v_o \Delta i_o}{8 f_s} \tag{18}$$

During other half cycle, the converter delivers energy directly to the load, and the capacitor is charged. The resulting change in the energy given by

$$\Delta E_2 = C_o v_o \Delta v_o. \tag{19}$$

In order to keep the DC voltage constant, the changes in the energy during these cycles must be equal, leading to

$$C_o = \max\left\{\frac{\Delta i_o}{8 f_s \Delta v_o}\right\} \tag{20}$$

Considering the worst case scenario, the value for the output capacitance is $C_o = 8.33\ \mu F$, resulting in a reduced size and volume output filter, compared with the alternative DC-DC conversion stages.

Table 2. Simulation parameters for fast charger

Parameter	Value
Rated Power	$240\ kW$
Total DC-link Voltage	$2000\ V$
switching frequency	$2\ kHz$
Output Filter Inductance	$10.4\ mH$
Output Filter Capacitance	$8.3\ \mu F$
Output DC Voltage Range	$300 - 600\ V$
Proportional Gain	0.1089
Integration Time	$0.15\ \ s$

5.2 Simulation Results

With the aforementioned control strategy and controller parameters, the proposed fast charger configuration is simulated in MATLAB/Simulink environment with the parameters listed in Table 2. For the moment, the rectifier stage and the grid connection are neglected and only the DC-DC stage is simulated assuming an ideal DC source. The load model is assumed to be resistive to simplify the analysis. The control of each buck converter is performed using a linear PI controller, which regulates the output current through the generation of a proper duty cycle.

Figures 14 and 15 show the interleaved and total output current of the DC-DC buck converter under steady state and transient operation. The interleaving operation effectively triplicates the equivalent switching frequency and reduces the total output current ripple. By analyzing the currents generated in each converter branch of Figure 14, it is possible to see that each branch is contributing one third of the total output current. However, due to the harmonic cancellation by interleaving the buck converter, the total output current presents a lower ripple, which is within the limits imposed and an equivalent frequency of 6 kHz, this multiplicative effect allows use of a small output filter and still meet the secure battery charging requirements.

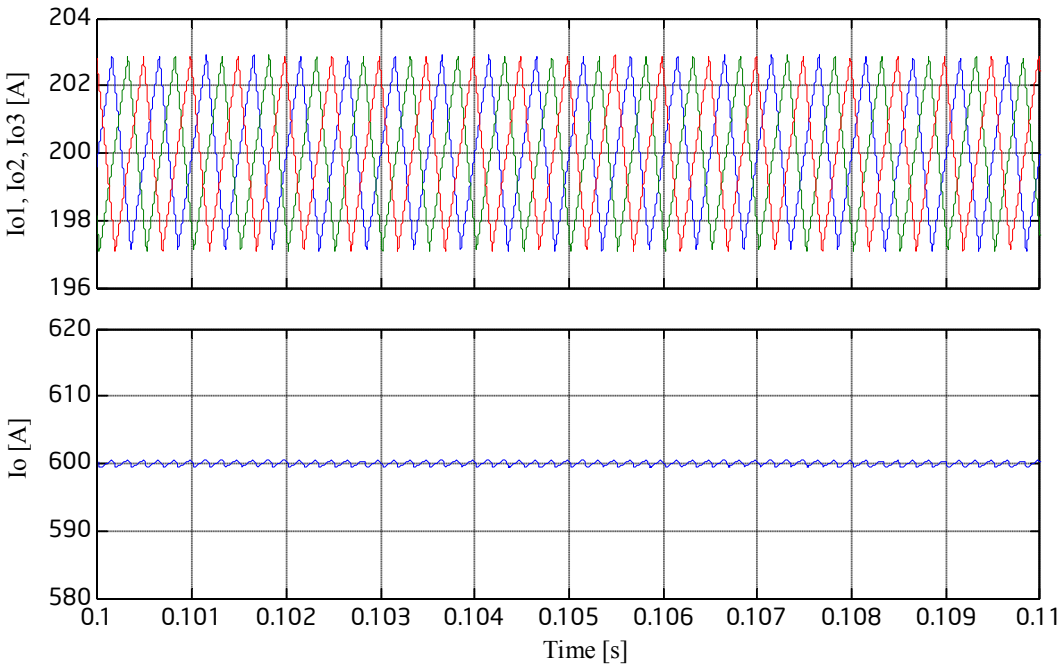

Figure 14. Individual and total output currents of interleaved buck converters under steady state.

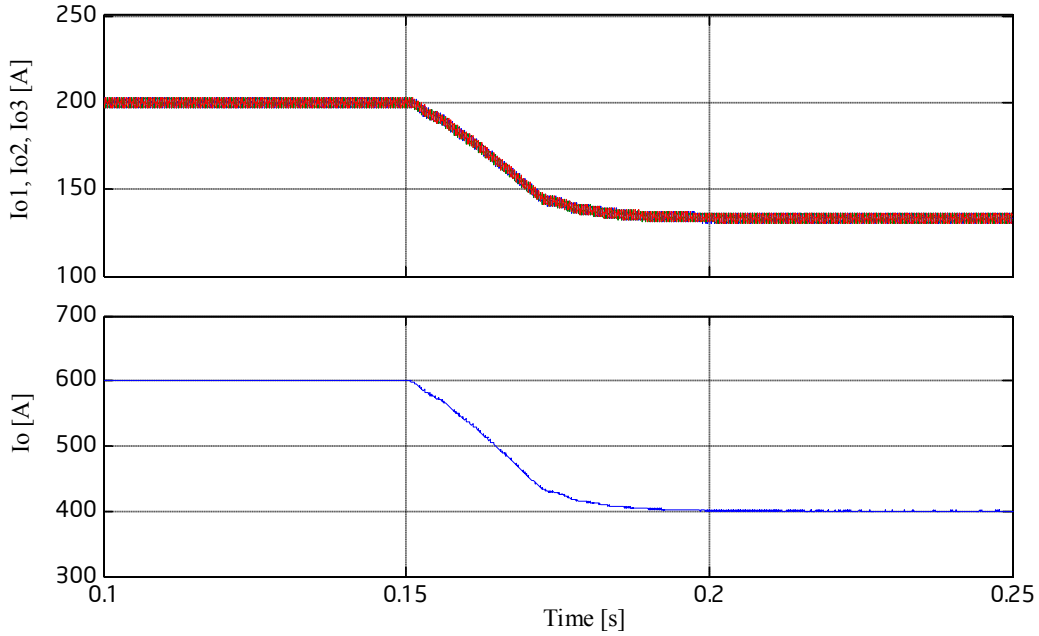

Figure 15. Individual and total output currents of interleaved buck converters under transient operation.

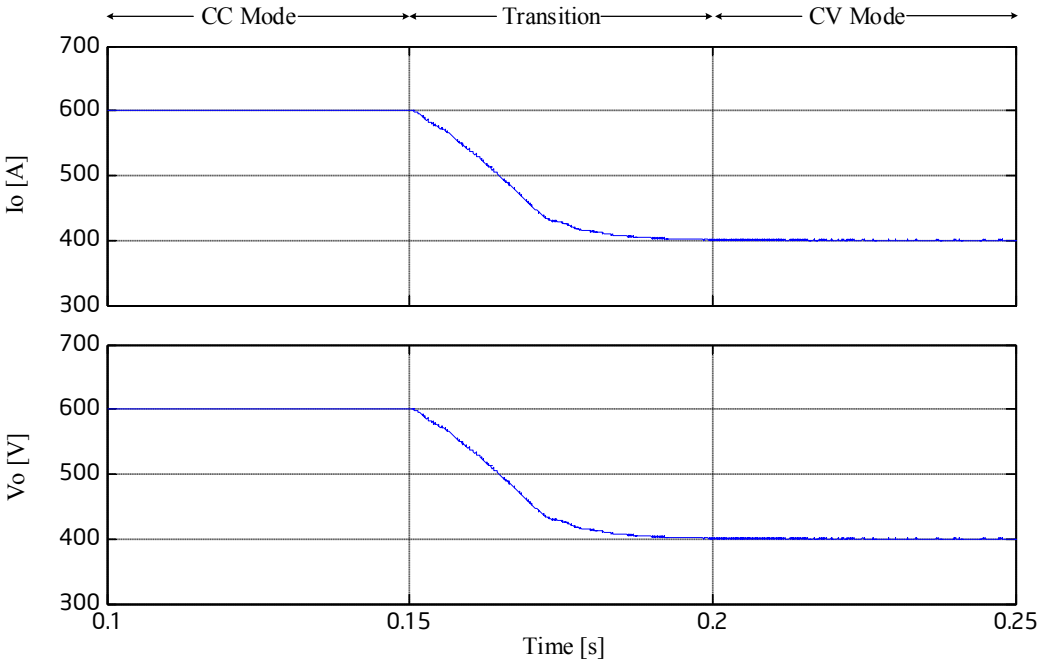

Figure 16. Converter output current and voltage during transition from CC to CV charging mode.

Figure 16 gives the battery voltage and current waveforms during a transition from CC mode to CV charging mode. Prior to 0.15 s, the charger is under CC mode and the battery is charged

with a constant current. After transition at 0.15 s, the controller switches to cascaded control loop. The outer voltage loop starts to act and regulates the battery voltage at a constant level. In addition, Figure 16 shows a smooth DC output with a reduced ripple value, thereby confirming the previous design procedure and analysis.

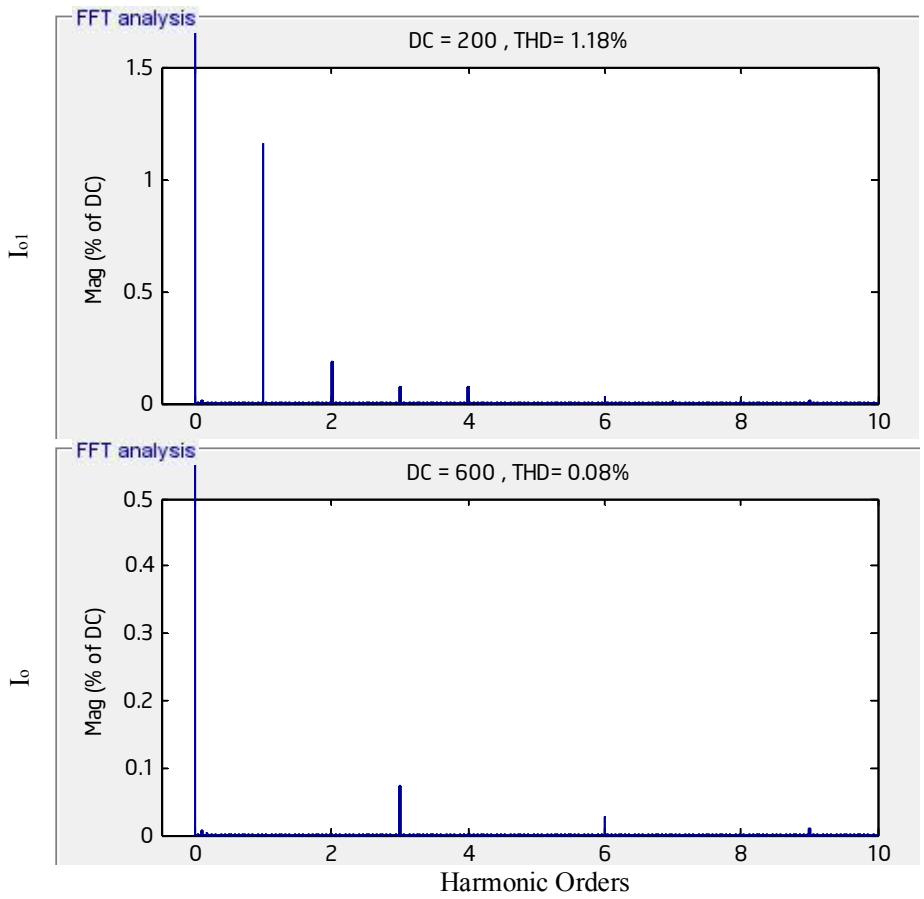

Figure 17. FFT analysis for DC-DC converter output current.

In order to highlight the advantages of the proposed topology, Figure 17 presents the fast Fourier transform (FFT) analysis on the DC-DC converter output current. The harmonic analysis is carried out at 200 A and 600 A output current. The waveforms clearly exhibit the harmonic cancelation obtained by the multi-phase buck converter. The main harmonics of the total output current locates at 6 kHz, which is three times of the main harmonics of each branch output current. It also confirms that the output current harmonic profile do not contain any harmonics at $6n \pm 1$ harmonic order.

5.3 Experimental Results

In order to verify the proposed interleaved buck converter based fast charger and its charging control further, a scale-down prototype is built. The main parameters of the fast charger are shown in Table 3. The overview picture of the prototype is shown in Figure 18, and the main digital control platform for fast charger is presented in Figure 19, which utilizes the DSPTMS320F28335 to realize core algorithms, and also a FPGA to deal with peripheral logics such as protection, communication, etc.

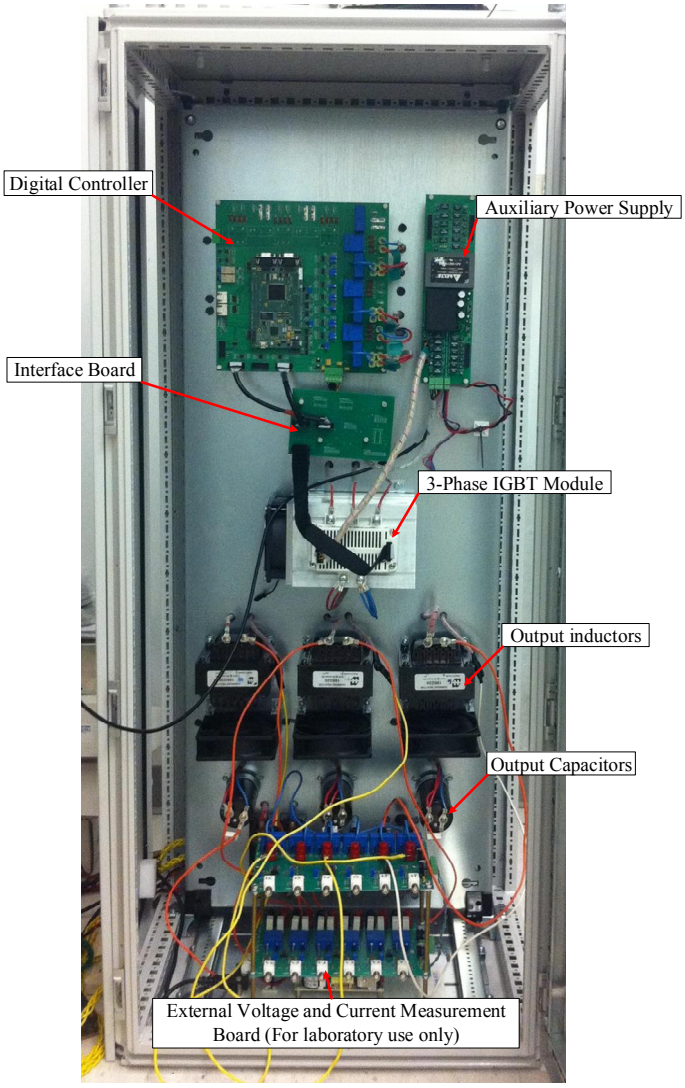

Figure 18. Photograph of fast charger prototype.

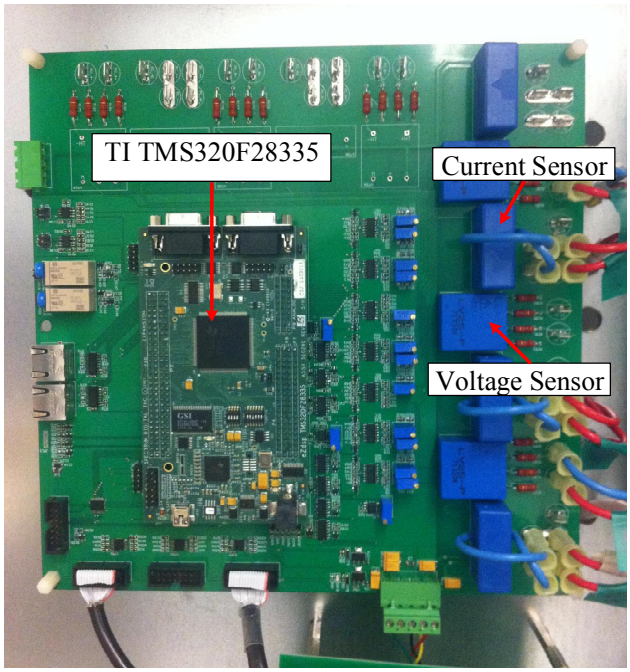

Figure 19. Photograph of main digital controller platform.

Figures 20 and 21 present the transition process from CC mode (i_o = 18 A) to CV mode (v_o = 90 V), while Figures 22 and 23 demonstrate the transition process from CV mode (v_o = 90 V) to CC mode (i_o = 18 A). The experimental results verify that the transition between CC and CV modes is smooth. The controller design and simulation results in previous sections are therefore well supported by the experimental results.

Table 3. Parameters of low-power fast charger prototype.

Parameter	Value
Rated Power	$5\ kW$
dc-link Voltage	$230\ V$
Device switching frequency	$5\ kHz$
Output Filter Inductance	$5\ mH$
Output Filter Capacitance	$3000\ \mu F$
Output DC Voltage Range	$50 - 200\ V$

Figures 24 and 25 show the steady experimental waveforms under CC mode and CV mode, respectively. Similar to simulation results, due to the harmonic cancellation by interleaving the buck converter, the total output current presents a much lower ripple.

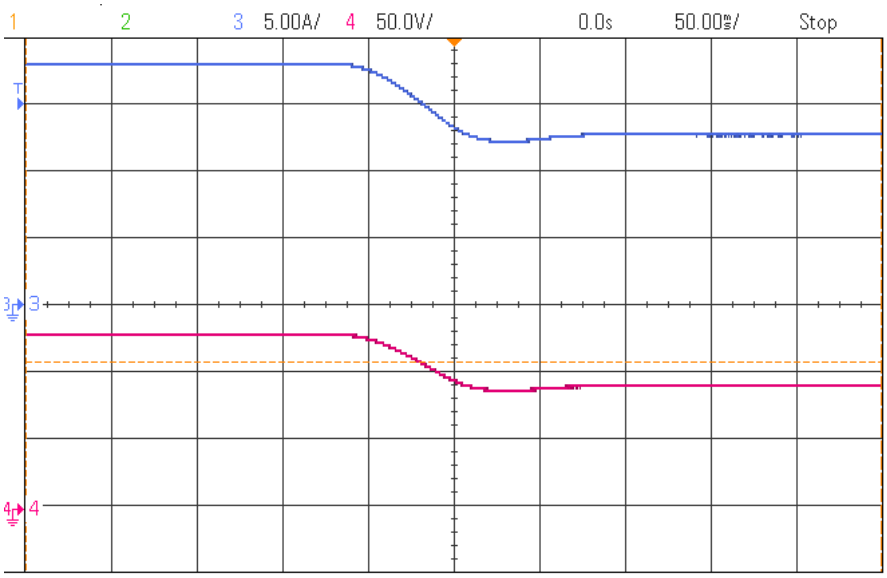

Figure 20. Experimental results for converter output current and voltage during transition from CC mode (i_o=18 A) to CV mode (v_o=90 V). Ch3: total output current (5 A/div), Ch4: output voltage (50 V/div), Time scale: 50 ms/div.

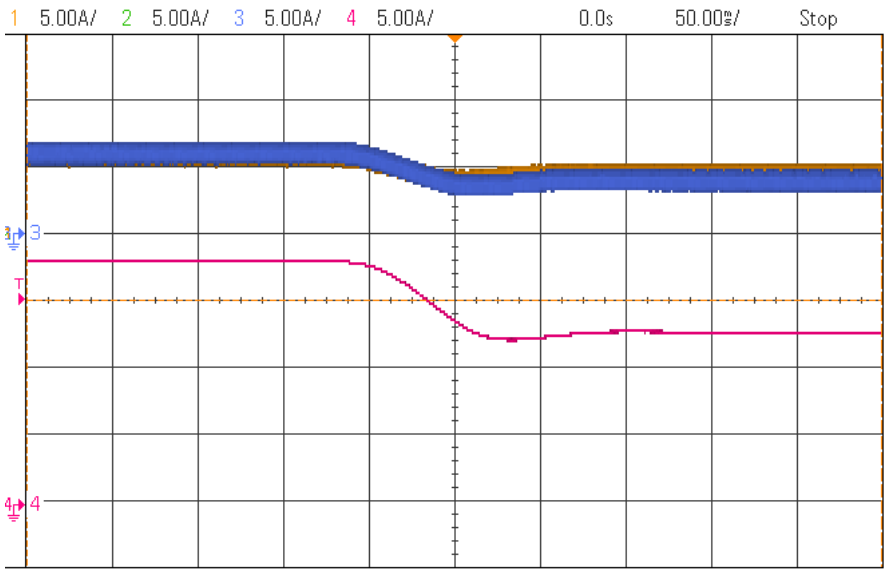

Figure 21. Experimental results for individual channel currents and total output current during transition from CC mode (i_o=18 A) to CV mode (v_o=90 V). Ch1-Ch3: three units output currents (5 A/div), Ch4: total output current (5 A/div), Time scale: 50 ms/div.

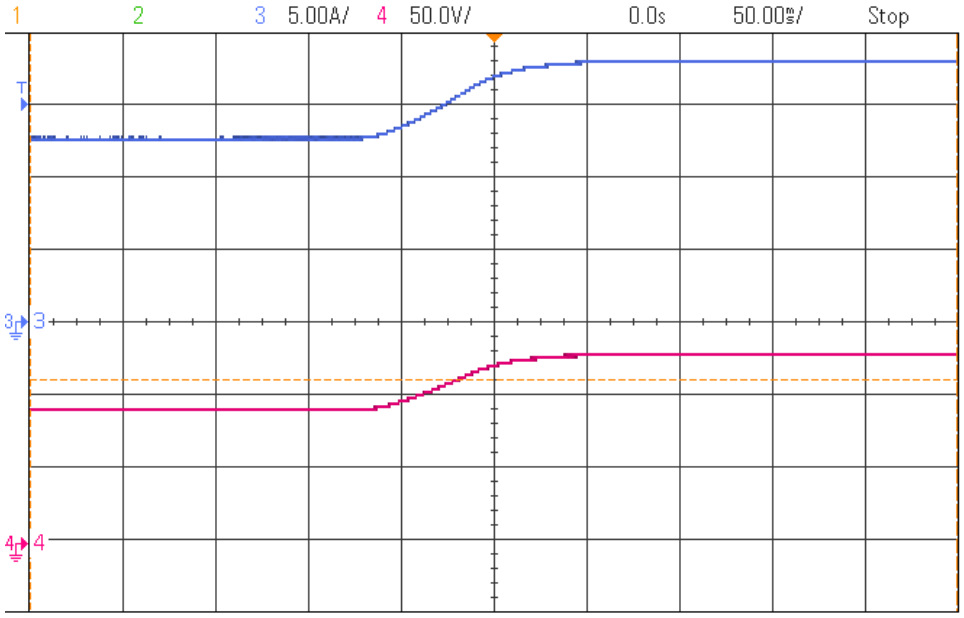

Figure 22. Experimental results for converter output current and voltage during transition process from CV mode (v_o=90 V) to CC mode (i_o=18 A). Ch3: total output current (5 A/div), Ch4: output voltage (50 V/div), Time scale: 50 ms/div.

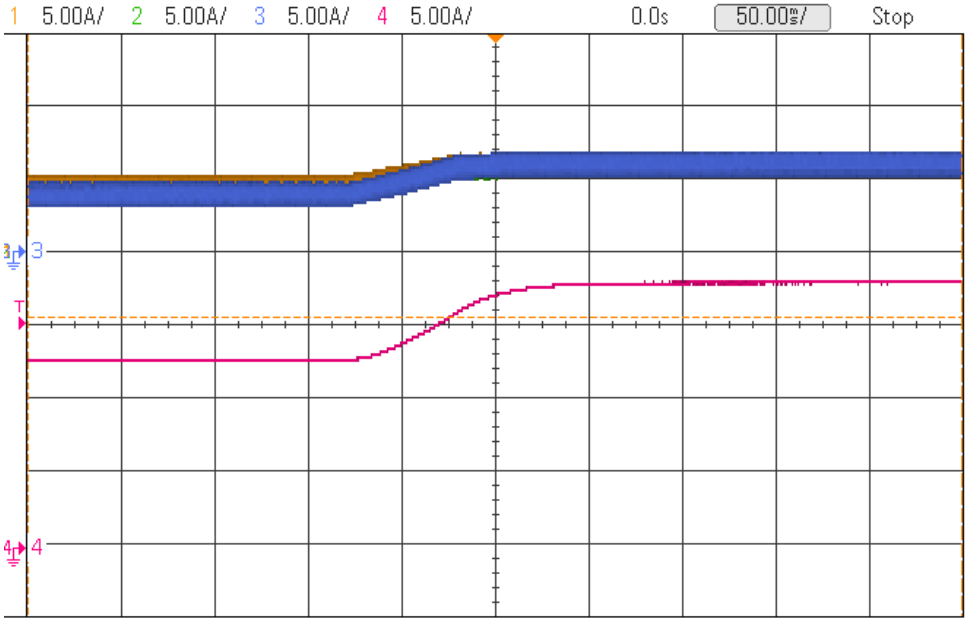

Figure 23. Experimental results for individual channel currents and total output current during transition process from CV mode (v_o=90 V) to CC mode (i_o=18 A). Ch1-Ch3: three units output currents (5 A/div), Ch4: total output current (5 A/div), Time scale: 50 ms/div.

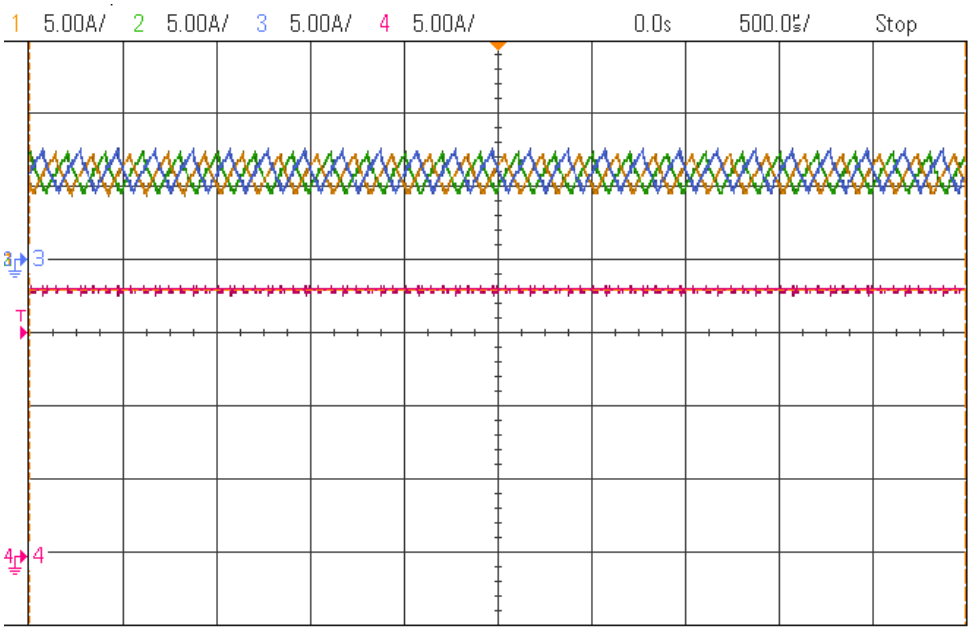

Figure 24. Experimental results for individual channel currents and total output current during CC mode (i_o=18 A). Ch1-Ch3: three units output currents (i_{o1}-i_{o3}) (5 A/div), Ch4: total output current (5 A/div), Time scale: 500 us/div.

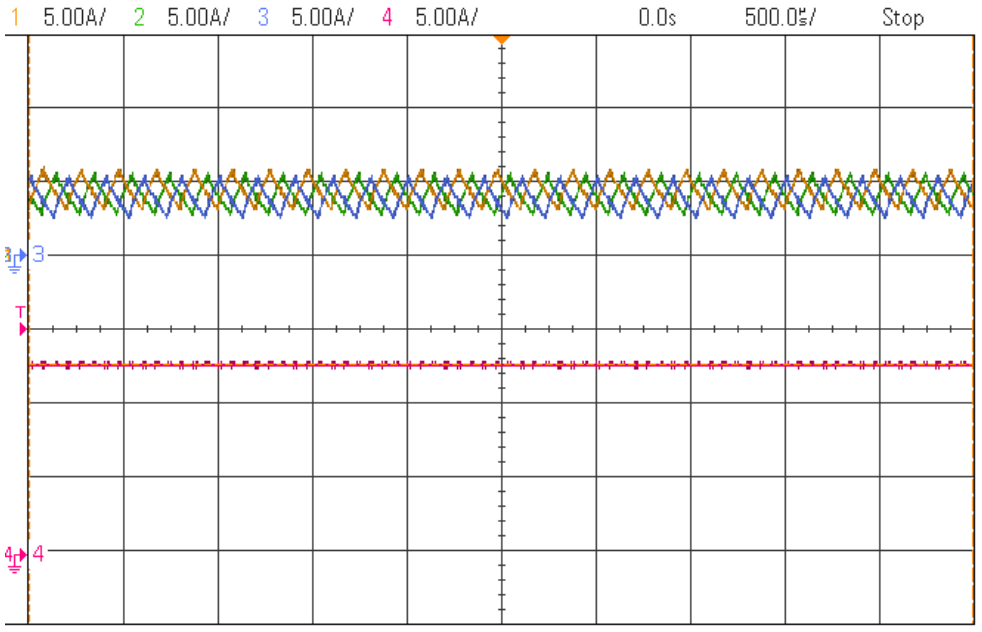

Figure 25. Experimental results for individual channel currents and total output current during CV mode (v_o = 90 V). Ch1-Ch3: three units output currents (i_{o1}-i_{o3}) (5 A/div), Ch4: total output current (5 A/div), Time scale: 500 us/div.

6 Conclusions

In this report, Level III fast charger is discussed through theoretical analysis, design procedure, and simulation and experimental tests. The use of multi-phase interleaved buck converters allows the generation of smooth DC output without the need of bulky filter inductors or capacitors. With the proposed converter topology, harmonic cancellation in the DC-DC converter output current has been achieved by employing interleaved (phase-shift) operation. This leads to output currents and voltages with reduced ripple values and a multiplicative effect on the equivalent output frequency.

For the fast charging application, where high output currents are needed to shorten the charging time, the multi-phase interleaved buck converter is a promising candidate to share the high charging currents between multiple modules. It is easy and convenient to scale up the power rating by increasing parallel units. Simulation and experimental results have been presented during CC and CV modes to verify the effectiveness of the proposed interleaved buck converter and its closed-loop digital control scheme.

7 Publications

In addition to the laboratory prototype developed, this project has resulted in 5 scholarly publications including 3 journal papers in high-impact factor IEEE journals, and 2 IEEE conference papers. One journal paper has been accepted for publication by the *IEEE Transactions on Power Electronics* (impact factor = 6.008), and the other two journal papers have been submitted for review to the *IEEE Transactions on Industrial Electronics* (impact factor = 6.498). One conference paper has been published in the *10th IEEE Conference on Industrial Electronics and Applications (ICIEA 2015)*, while another conference paper has been submitted to the *41st Annual Conference of IEEE Industrial Electronics Society (IECON2015)*. The summary of research publications is given below:

[1]. L. Tan, B. Wu, S. Rivera, and V. Yaramasu, "Comprehensive DC Power Balance Management in High-Power Three-Level DC-DC Converter for Electric Vehicle Fast Charging," IEEE Transactions on Power Electronics., vol. PP, no. 99, pp. 1–1, 2015. (Accepted for publication)

[2]. L. Tan, B. Wu, V. Yaramasu, and S. Rivera "Effective Voltage Balance Control for Bipolar-DC-Bus Fed EV Charging Station with Three-level DC-DC Fast Charger", submitted to IEEE Transactions on Industrial Electronics, 2015. (In peer-review process)

[3]. L. Tan, B. Wu "Novel Integrated Inductor for Eliminating Circulating Current of Parallel Three-level DC-DC Converter based EV Fast Charger" submitted to IEEE Transactions on Industrial Electronics, 2015. (In peer-review process)

[4]. L. Tan, B. Wu, V. Yaramasu, and S. Rivera "Effective Voltage Balance Control for Three-Level Bidirectional DC-DC Converter Based Electric Vehicle Fast Charger" ICIEA 2015, pp. 1-6, New Zealand, June 2015. (Accepted for publication)

[5]. L. Tan, B. Wu, and S. Rivera "Novel Bipolar-DC-Bus EV Fast Charging Station with Intrinsic DC-Bus Voltages Equalization and Minimized Voltage Ripples" submitted to IECON, Japan, 2015. (Accepted for publication)

8 References

[1] M. Hajian, H. Zareipour, and W. D. Rosehart, "Environmental benefits of plug-in hybrid electric vehicles: The case of Alberta," in Proc. IEEE Power & Energy Society General Meeting, pp. 1–6, 2009.

[2] J. F. Kevin Morrow, Donald Karner, "Plug-in Hybrid Electric Vehicle Charging Infrastructure Review," Fin. Rep., Battelle Energy Alliance, p. 40, 2008.

[3] A. S. Charles Botsford, "Fast Charging vs. Slow Charging Pros and Cons for the New Age of Electric Vehicles," in P roc. 24th Electric Vehicle Symposium, Norway, p. 9, 2009.

[4] L. Dickerman and J. Harrison, "A New Car, a New Grid," IEEE Power and Energy Mag., vol. 8, no. 2, pp. 55–61, 2010.

[5] B. Sanzhong and S. M. Lukic, "Unified Active Filter and Energy Storage System for an MW Electric Vehicle Charging Station," IEEEE Trans .Power Electron., vol. 28, no. 12, pp. 5793–5803, 2013

[6] "SAE Charging Configurations and Ratings Terminology," *SAE Hybrid Committee, http://www.sae.org/smartgrid/chargingspeeds.pdf,* 2011.

[7] "SAE Surface Vehicle Recommended Practice J1772, SAE Electric Vehicle Conductive Charge Coupler," *SAE International,* 2010.

[8] C. Botsford and A. Szczepanek, "Fast charging vs. slow charging: Pros and cons for the new age of electric vehicles," *EVS24, Stavanger, Norway,* 2009.

[9] L. Demas, T. A. Meynard, H. Foch, and G. Gateau, "Comparative study of multilevel topologies: NPC, multicell inverter and SMC with IGBT," in *IECON 02 [Industrial Electronics Society, IEEE 2002 28th Annual Conference of the]*, 2002, pp. 828-833 vol.1.

[10] Y. Gurkaynak and A. Khaligh, "Control and Power Management of a Grid Connected Residential Photovoltaic System with Plug-in Hybrid Electric Vehicle (PHEV) Load," in *Applied Power Electronics Conference and Exposition, 2009. APEC 2009. Twenty-Fourth Annual IEEE*, 2009, pp. 2086-2091.

[11] S. Dusmez, A. Cook, and A. Khaligh, "Comprehensive analysis of high quality power converters for level 3 off-board chargers," in *Vehicle Power and Propulsion Conference (VPPC), 2011 IEEE*, pp. 1-10.

[12] D. Aggeler, F. Canales, H. Zelaya-De La Parra, A. Coccia, N. Butcher, and O. Apeldoorn, "Ultra-fast DC-charge infrastructures for EV-mobility and future smart grids," in *Innovative Smart Grid Technologies Conference Europe (ISGT Europe), 2010 IEEE PES*, pp. 1-8.

[13] T. Hegarty, "Benefits of multi-phasing buck converters," *EE Times-India,* 2007.

9 Appendix: user manual for bidirectional fast charger

9.1 Fast charger prototype system

To verify the performance of proposed fast charger, one scale-down 5kW prototype system is designed. One IGBT module, IFS150V12PT4, is used for the 3-phase buck converter. The main controller is based on DSP (TMS320F28335) and FPGA (EP1C6T144C8), which samples the output currents and output voltage, then through proposed algorithms and interleaved PWM methods, the PWM signals are generated to control the 3-phase buck converter. The parameters of the prototype are shown in Table. 3. The schematic diagram and real picture of fast charger prototype are shown in Figure 26, the component details of which can be found in Figure 18.

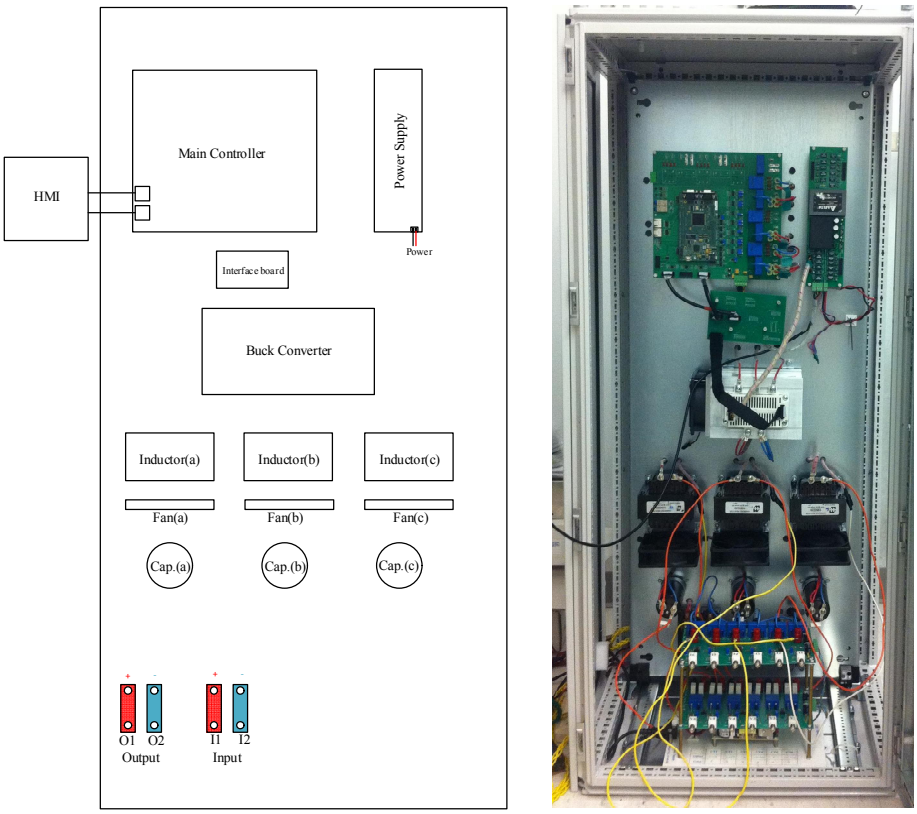

(*a*) Schematic Diagram (*b*) Real Picuture

(*a*). Schematic diagram. (*b*). Real picture.

Figure 26. Schematic diagram and real picture of fast charger prototype.

9.2 HMI board.

As shown in Figure 27, the HMI board is composed of 1 LCD screen, 24 small buttons, and 2 Ethernet ports which are connected with the main controller board. The communication between HMI board and main controller board is based on two FPGAs on the two boards. Only three buttons have been used to control the operation of fast charger, which are "**Del**", "**Enter**", and "**Home**", corresponding to "Reset errors", "Start running", and "Stop running".

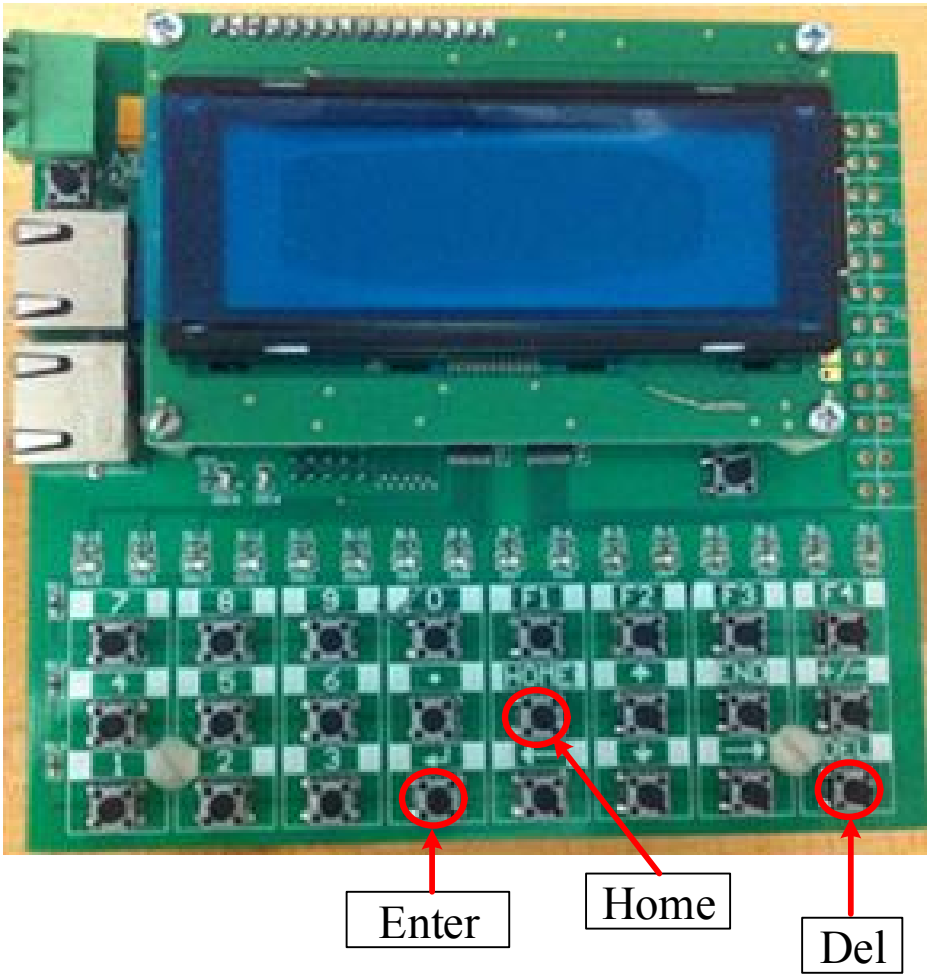

Figure 27. Real picture of HMI board.

9.3 Procedures to run the fast charger.

1). Make sure the input of fast charger connected to the output of a charging station or to the output of a DC power supply. (Refer to the instructions in Figure 26.)

2). Make sure the output of the fast charger connected to a load, such resistors or batteries.

3). Put the power plug of the power supply board into one socket on the wall to power on the main controller board.

4). Reset all possible failure signals by pressing the "**Del**" button of the HMI board.

5). Run the charging station to supply DC voltages, or turn on the switch on the wall to connect the DC power supply (Tune the output to be around 230V).

6). Press "**Enter**" button of the HMI board to start the fast charger.

9.4 Procedures to stop the fast charger.

1). Press "**Home**" button of the HMI board to stop the fast charger.

2). Disconnect the fast charger to the charging station, or turn off the switch on the wall to disconnect the DC power supply.

3). Disconnect the power plug of the power supply board.

4). Close the door of the fast charger cabinet.